Ion shell distributions as free energy source for plasma waves on auroral field lines mapping to plasma sheet boundary layer

A. Olsson[1], P. Janhunen[2], and W.K. Peterson[3]

[1]Swedish Institute of Space Physics, Uppsala Division, Uppsala, Sweden
[2]Finnish Meteorological Institute, Geophysical Research, Helsinki, Finland
[3]LASP, University of Colorado, Boulder, Colorado, USA

Camera-ready Copy for

Annales Geophysicae

Manuscript-No. ???

Annales Geophysicae (20**) *:101–117

Ion shell distributions as free energy source for plasma waves on auroral field lines mapping to plasma sheet boundary layer

A. Olsson[1], P. Janhunen[2], and W.K. Peterson[3]

[1]Swedish Institute of Space Physics, Uppsala Division, Uppsala, Sweden
[2]Finnish Meteorological Institute, Geophysical Research, Helsinki, Finland
[3]LASP, University of Colorado, Boulder, Colorado, USA

Received: ??? – Accepted: ???

Abstract. Ion shell distributions are hollow spherical shells in velocity space that can be formed by many processes and occur in several regions of geospace. They are interesting because they have free energy that can, in principle, be transmitted to ions and electrons. Recently a technique has been developed to estimate the original free energy available in shell distributions from in-situ data where some of the energy has already been lost (or consumed). We report a systematic survey of three years of data from the Polar satellite. We present an estimate of the free energy available from ion shell distributions on auroral field lines sampled by the Polar satellite below 6 R_E geocentric radius. Our analysis shows that ion shell distributions that have lost some of their free energy are commonly found in the evening sector auroral field lines. We suggest that these "partially consumed shell distributions" are formed during the so called Velocity Dispersed Ion Signatures (VDIS) events. Furthermore we find that the partly consumed shells often occur in association with enhanced wave activity and middle-energy electron anisotropies. The maximum downward ion energy flux associated with a shell distribution is often 10 mW m^{-2} and sometimes exceeds 40 mW m^{-2} when mapped to the ionosphere and thus may be enough to power many auroral processes. Earlier simulation studies have shown that ion shell distributions can excite ion Bernstein waves which in turn energise electrons in the parallel direction. It is possible that ion shell distributions are the link between the X-line and the auroral wave activity and electron acceleration in the energy transfer chain for stable auroral arcs.

1 Introduction

Ion shell distributions are spherical shells in velocity space. They can be formed by many processes of which the most widely studied is the pickup process which occurs when the solar wind protons undergo a charge-exchange reaction with almost stationary neutrals. The slow ion resulting from the charge exchange is accelerated (picked up) by the solar wind electric field. Each ion will have the same magnitude of the velocity and after some pitch angle scattering process the other velocity components are randomised, resulting in a shell distribution. This mechanism has been studied in different context, including comets (Karimabadi et al., 1994) and the termination shock of the heliosphere (Kucharek and Scholer, 1995).

Inside the magnetosphere, shell distributions have not yet been studied much. Bingham et al. (1999), referring to Freja data published by Eliasson et al. (1994), discussed hot ion shell distributions with a loss cone at low altitude (which they called horseshoe distributions) and found that such distributions can generate lower hybrid waves. Ion shell distributions with dual loss cones have been discussed by Engebretson et al. (2002). They noted that these double loss cone distributions (which have been called toroidal by some investigators) at sub-auroral latitudes are maintained by transport from the plasma sheet and are possibly the free energy source of various pulsation modes. Janhunen et al. (2002) provided examples of shell distributions in auroral latitudes at $\sim 4-5R_E$ radial distance (geocentric distance) using Polar/TIMAS data and showed with the help of solving the linear dispersion relation numerically and by using a two-dimensional particle simulation that the observed shell distribution is unstable to a broad range of ion Bernstein wave modes. It was also shown in the paper that the generated Bernstein waves accelerate $\sim$ 100 eV electrons at a rate of $\sim$ 80 eV/s. More important for this report is that Janhunen et al. (2002) have developed a technique to estimate the original free energy available in shell distributions form in-situ data where some of the energy has already been transformed (or consumed).

Velocity-dispersed ion signatures (VDIS) have been studied in the plasma-sheet boundary layer (PSBL) by many authors (Elphic and Gary, 1990; Baumjohann et al., 1990; Zelenyi et al., 1990; Bosqued et al., 1993a,b; Onsager and Mukai, 1995). By VDIS one refers to events in the PSBL where the ion energy increases towards the polar cap boundary when measured by a satellite traversing through the auroral zone towards increasing latitude. The origin of the VDIS ions is assumed to be the reconnection X-line, and VDIS energy-latitude slopes have been used to find the location of the X-line, for example Zelenyi et al. (1990). The three-dimensional ion distribution function corresponding to VDIS has not been directly addressed in the literature. Our analysis suggests that the ion shell distributions seen in the Polar/TIMAS 6 R_E radial distance in the PSBL form a VDIS when considered in the energy-latitude plane.

The main emphasis of the paper is in the PSBL ion shells. In addition to the PSBL, it is found that shell distributions also occur in plasma sheet field lines and in the radiation belts. In order to meaningfully discuss the properties of PSBL shells, it is necessary to also present some of the properties of radiation belt shells. Physical causes and effects of radiation belt shells are outside the scope of the paper, however. Separate papers should be reserved for these important topics.

Our motivation for studying shell distributions in the auroral zone is that such distributions contain a lot of free energy. Janhunen et al. (2002) have shown that wave modes exist in the region which can tap this free energy. They have also developed a technique to estimate the available free energy available from in-situ data. If significant tapping of the shell distribution free energy takes place, the total power transferred through shell distributions to waves and later to the electrons may be sufficient for powering some visible auroral features.

The structure of the paper is as follows. After describing the relevant Polar satellite instruments and data processing we approach the ion shell distributions from different viewpoints. The first two viewpoints (sections 4 and 5) deal with basic statistical properties of the free energy available on auroral field lines from ion shells. In section 6 we present a visual categorisation of auroral zone ion shells with examples. Then the behaviour of ion shell free energy and the correlation of ion shells with electron anisotropies and waves is analysed. The paper ends with a summary and discussion.

2 Instrumentation

The Polar satellite has the advantage of having three years of measurements of both ions and electrons as well as wave electric fields. The results of Janhunen et al. (2002) have motivated this investigation. The existence of the Polar data base makes it possible to systematically investigate correlations between ion shell distributions, electron anisotropy and waves. We use summary Polar/TIMAS ion data from 1996-1998 (Shelley et al., 1995) archived at the NASA Space Science Data Center for identifying and characterising ion shell distributions. The energy range is between 15 eV and 33 keV and time resolution about 12 s (corresponding to two spin periods). The differential energy flux for the ions is produced in 15 $^{\mathrm{o}}$ bins for all pitch angles. Ion data exists after 1998, however, a high-voltage breakdown in TIMAS in 8 December 1998 caused a loss of sensitivity in the data and makes it very challenging to mix data from before and after this date.

During the same time period as for the ion data i.e. 1996-1998, the wave electric fields in the 1-10 Hz frequency range are available from the Polar Electric Field Instrument, EFI, (Harvey et al., 1995). Polar EFI makes 3-D measurements with a sampling rate of 20 samples per second. We exclude spin axis measurements in this study due to uncertainties in the measurements from the short boom (5 m) in this direction. We make the assumption that the spin axis component of the electric field is negligible in the auroral zone since the spin axis is in the east-west direction here. The parallel and perpendicular wave electric fields will be estimated with the help of the Polar Magnetic Field Experiment (MFE) (Russell et al., 1995).

To investigate the electron anisotropy from the electron distribution function we use the Level-0 Polar HYDRA electron data (Scudder et al., 1995). The energy range of the data is 2 eV-28 keV and the time resolution is about 12 seconds.

In one event we also plot, in addition to EFI spectrogram, a spectrogram from the plasma wave instrument PWI (Gurnett et al., 1995).

Polar data from the time period 1996-1998 cover the altitude ranges 5000-10000 and 20000-32000km.

3 Data processing

3.1 Estimate of free energy and downward energy flux from TIMAS

The Polar/TIMAS instrument measures the differential number flux from which the differential energy flux and the distribution function can be obtained by multiplication and division by energy, respectively. In this study we are especially interested in the free energy and the downward total-ion energy flux for ion shell distributions. As described by Janhunen et al. (2002) we define the free energy of a given distribution function as the subtraction between the kinetic energy of the original distribution and the kinetic energy of the "closest" equilibrium distribution. The closest equilibrium distribution is found by a flattening procedure, which is repeated until no positive slopes are found in the distribution function . As discussed by Janhunen et al. (2002) and further below this procedure results in a a lower limit estimate of the free energy available.

The total-ion downward energy flux is obtained from the differential energy flux by integration over all pitch angles.

3.2 Wave electric fields from EFI and MFE

The EFI electric field was decomposed into parallel and perpendicular components by using spin-resolution (6 s) MFE data. We use frequencies in the 1-10 Hz range. The upper limit is dictated by the EFI instrument which produces 20 samples per second in its usual mode. The wave amplitudes are averaged to the same 12 s time resolution as the particle data.

3.3 Anisotropy from HYDRA

Electron anisotropy is most commonly defined in terms of parallel and perpendicular temperatures. However, in this study we will especially discuss a subrange of electron energy (100-1000 eV) whence it is more convenient to define the anisotropy in terms of density. We define the anisotropy as the partial density corresponding to the part of the electron distribution function from which a symmetrised perpendicular distribution function has been subtracted and the integration in velocity space is carried out between energies 100 eV and 1 keV only. For a detailed discussion on our employed definition of the anisotropy see Janhunen et al. (2003a), equations 2-4. Statistical results for the MLT-ILAT dependence of the anisotropy of electrons in the energy range 100-1000 eV in the auroral zone can be found in Janhunen et al. (2003a).

4 Free energy of ion shells: dependence on MLT-ILAT and Kp

To obtain general knowledge about how common and what type of phenomena the ion shell distributions are, we show statistics of their associated free energy in the MLT-ILAT plane in Figure 1 for all radial distances put together (1-6 R_E). The left subplot shows low Kp (Kp ≤ 2) and the right subplot high Kp (Kp > 2). Panel a shows the orbital coverage in hours, i.e. the number of hours the instrument was measuring in each MLT-ILAT bin. Panel b is the occurrence frequency of 12-s data points where the ion free energy exceeds the value 0.02 keV/cm^{-3}, while the 95-percentile is shown in panel c. The 95-percentile is defined as the value which is such that 95 % of the measured values of the free energy are smaller than the plotted value in each MLT-ILAT bin and 5 % are larger. Data points when no free energy is found in the distribution are counted as zero. We first discuss features which are common to low and high Kp. It is noteworthy that the occurrence frequency of the free energy exceeding 0.02 keV/cm^{-3} (Figure 1, panel b) is highest (0.4) in the radiation belt regions and lowest in the auroral zone (0.1) which is seen as almost white. From panel c, we see that statistically, the ion shells in the radiation belt are energetic having values of the free energy density around 0.1 keV/cm^{-3} in 5 % of the cases, while lower values (below 0.05 keV/cm^{-3}) of the free energy is found in the auroral zone.

The ion shell distributions in the radiation belt region are thus a common phenomenon. From looking at the individual radiation belt events one discerns that the ions are energetic (above 15 keV), and the distributions are stable, i.e. their free energy is not consumed. A typical example of an ion shell in the radiation belt is shown in Figure 2.

Ion shells in the auroral zone usually have lower ion energies than in the radiation belt, usually below 10 keV (Figure 3). For midnight MLT (22-02) one can see in Figure 1, panels b and c that the occurrence frequency of auroral ion shells (with free energy above 0.02 keV/cm^{-3}) is highest in latitudes corresponding to the part of the auroral zone adjacent to the polar cap (from ILAT ~ 68). Probably these ion shells originate from the PSBL and we will therefore refer to these ion shells as PSBL ion shells. In some events one sees ion shells also between the PSBL and the radiation belt; this may be either a genuine effect or be caused by auroral oval motion while the satellite is crossing it.

We now discuss the Kp differences seen in Fig. 1. The differences are small in the radiation belt. In the auroral zone, the free energy density is somewhat higher for high Kp and it is spread more uniformly over the MLT sectors 20-04, while for low Kp it is more concentrated in the midnight sector (22-02 MLT).

Typically, many of the ion shell distributions in the polar cap boundary and in the auroral zone (for 1-6 R_E) are partly flattened out. As an example, Figure 4 shows a half-consumed ion shell: the downgoing part is an ion shell but the upgoing part is a plateau. A natural idea is that the plateau in the upgoing part is due to wave-particle interactions which have consumed the free energy of the downgoing ion shell. In the case of a half-consumed ion shell the consumption process should occur below the measurement point.

5 Original free energy of ion shells: dependence on MLT-ILAT and Kp

If the ion shell distribution free energy is consumed by wave-particle interactions, a plateau is expected to be left at and near the energy range where a positive slope existed before. Plateaus in the ion distribution are therefore possible markers of free energy that has existed in the original distribution and that was subsequently consumed. If it is possible to reconstruct the original distribution from the plateaued one approximately, it is then possible to estimate its original free energy.

To automatically find the plateau distributions we use the kurtosis of the distribution (Press et al., 1992). Let us first define the nth moment M_n of the distribution function $f(v,\theta)$ by

$$M_n = 2\pi \int_{v_1}^{v_2} dv \int_0^{\pi} d\theta \sin\theta v^{n+2} f(v,\theta) \quad (1)$$

Here v_1 and v_2 define the energy range over which the integration is carried out (see below). Then the kurtosis K is defined by (Press et al., 1992)

$$K = \frac{M_0 M_4}{M_2^2} - 5/3. \quad (2)$$

The constant $5/3$ is subtracted to make K zero for a Maxwellian distribution. Notice that the kurtosis K is a dimensionless number. Plateau distributions are characterised by a negative kurtosis. Whenever K is negative, we define the "original" free energy density u_{orig} of the distribution by

$$u_{\mathrm{orig}} = (-K)\frac{1}{2} m_i M_2, \quad (3)$$

i.e. $(-K)$ times the total energy density of the distribution (m_i is the ion mass which is taken to be the proton mass).

There is no mathematical guarantee that Eq. (3) gives the original free energy of the distribution function, even approximately. On the contrary, one might criticise it on the grounds that for e.g. shell distributions, it gives results which in general differ from those obtained by the flattening procedure. However, Eq. (3) has the benefit that it is straightforward and relatively fast to compute and it satisfies the following basic requirements: (1) $u_{\rm orig}$ is linear in f, i.e. doubling the number of particles doubles the value of $u_{\rm orig}$, (2) $u_{\rm orig}$ is zero for a Maxwellian, (3) $u_{\rm orig}$ increases if the distribution becomes more plateau-like, (4) for a maximally plateaued step function distribution $-K = 10/21 \approx 0.476$ and for a delta function shell distribution it is $-K = 2/3$ so $u_{\rm orig}$ is always clearly less than the total energy density $(1/2)m_i M_2$.

There are cases where the distribution function is cusplike at one energy range (often at small energies) and plateau-like at some other energy range. The cusplike features contribute positive and the plateau-like features contribute negative kurtosis. Physically, we want possible existence of cusp-like ("Matterhorn-like") features in the distribution function not to decrease $u_{\rm orig}$. Therefore we use the following prescription. We set v_1 to correspond to 1 keV energy (we are not interested in shell distributions below 1 keV) and let v_2 vary from 5 keV to the maximum energy of the instrument which is 32 keV, compute $u_{\rm orig}$ in each case and take the maximum resulting $u_{\rm orig}$ to represent the "original" energy density of the distribution.

Figure 5 shows the statistical distribution of $u_{\rm orig}$ in the MLT-ILAT plane for low and high Kp. The format of the figure is similar to Fig. 1 which showed the MLT-ILAT distribution of the current free energy density u. Comparison of Figs. 1 and 5 yields two basic conclusions for both low and high Kp's: (1) while u (Fig. 1) is minimal in the auroral zone, $u_{\rm orig}$ (Fig. 5) is quite large there, (2) $u_{\rm orig}$ is also enhanced at subauroral latitudes in the postnoon sector. Conclusion (1) means that although ion shells do not contain very much free energy in the auroral zone on the average, the auroral zone is nevertheless full of plateaued distributions which may be interpreted as consumed ion shells. Notice that the auroral zone in general consists of discrete auroral features and the inactive regions between them, the latter usually dominating in area. Therefore, if the shell distributions are the "fuel" for stable discrete auroral features, at a given epoch the shell "burn" takes place only in thin layers corresponding to auroral arcs, but the rest of the region is filled with "auroral ash", i.e. the plateau distributions. The plateaus are destroyed by rather slow processes like large-scale convection that carries them away, velocity space diffusion and charge exchange reactions.

We now discuss how to understand conclusion (2) given in the previous paragraph, i.e. that $u_{\rm orig}$ is enhanced at subauroral latitudes in the postnoon sector. In Figure 6 we show drift paths of equatorial plane protons for different energies (1, 5, 10 and 20 keV), assuming a dipole magnetic field. The particles are launched at MLT 24. The drifts taken into account are the $\mathbf{E} \times \mathbf{B}$ drift and the gradient drift, the curvature drift is zero for equatorial particles. In the $\mathbf{E} \times \mathbf{B}$ drift, the corotation field and a constant duskward electric field of 0.1 mV/m magnitude are included. The 1 keV protons (panel a) show competition between the corotation drift and the gradient drift since they propagate eastward or westward, depending on their initial condition. At 5 and 10 keV (panels b and c) the particles drift westward due to the gradient drift, but exit from the magnetosphere near noon due to the duskward electric field. At 20 keV (panel d) the gradient drift is strong enough to keep the particles trapped so that they also propagate to the morningside. In TIMAS data, the intact, unconsumed shell distributions at low latitudes (radiation belt) are usually at high energies (more than 15 keV). As seen in panel d, such protons are trapped and are found at both prenoon and postnoon sectors. This is probably the reason why the free energy density plots (Fig. 1) are almost symmetrical in MLT about noon. The situation is different for the plateau distributions corresponding to the quantity $u_{\rm orig}$ shown in Fig. 5, however: these protons are usually at somewhat lower energies ($\sim$ 2-10 keV). According to Fig. 6, such protons exist only in the postnoon sector, thus this explains why $u_{\rm orig}$ is enhanced at subauroral latitudes in the afternoon sector but not in the morning sector.

We now discuss Kp differences in Fig. 5. On the morningside (0-12 MLT), the original free energy $u_{\rm orig}$ is clearly larger for high Kp than for low Kp in the auroral zone. On the eveningside (12-24 MLT) the increase with Kp concerns both auroral and radiation belt latitudes. At all MLT sectors, a weak tendency exists for the enhanced $u_{\rm orig}$ features to move towards lower ILAT for increasing Kp, which is probably due to the expansion of the polar cap for southward interplanetary magnetic field conditions, which are more common during high Kp than during low Kp. In general, the Kp effects are larger in $u_{\rm orig}$ (Fig. 5) than in u (Fig. 1). This indicates that stable, unconsumed shell distributions are rather insensitive to Kp variations at least in the radiation belt, but plateaued distributions (consumed shells) are more widespread in the auroral region for high Kp than for low Kp.

6 Categorisation of PSBL ion shells

When manually looking through individual PSBL shell distributions we have already mentioned that the ion shells often seem to be just partly shell-like, i.e. the ion shells have been partly consumed. To investigate whether there is a favourable altitude where the shells are consumed, we study how four different classes of ion shells vary with altitude.

To classify ion shell distributions by looking at the distribution function by eye, we use the following categorisation. In this categorisation we also make use of electron anisotropies and the electric component of 1-10 Hz waves. These two quantities have been found to be correlated with each other in the auroral region (Janhunen et al., 2001).

In Figure 7 we show Polar data from several instruments (upper subfigure) together with the TIMAS distribution function (lower subfigure). Before going into categorisation we explain the meaning of the panels in the upper subfigure. Panel a is EFI wave spectrogram showing electric wave activity. Panel b is a measure of electron anisotropy computed from HYDRA, the quantity shown is the measured differential flux in the parallel direction divided by the measured differential flux in the perpendicular direction (Janhunen et al., 2003a). $T_{\parallel} > T_{\perp}$ electron anisotropies are seen as red in panel b. Panel c shows the anisotropic part of the density for middle-energy (100-1000 eV) electrons only in red and the up minus down anisotropy in green. The quantities shown in panels b and c are defined more exactly in Janhunen et al. (2003a). Panels d and e are spectrograms for down and upgoing TIMAS ions, respectively. The quantity plotted is the differential energy flux for all ion species summed together. Panel f is the free energy density in keV cm^{-3} for TIMAS protons, computed by the flattening method mentioned above and defined in Janhunen et al. (2002). Finally, panel g shows the parallel energy flux for all TIMAS ions (positive upward). The energy flux has been mapped to the ionospheric plane, i.e. multiplied by the ratio of ionospheric versus local magnetic field and expressed in mW m^{-2}.

Category 0, full ion shells without electron anisotropy (Figure 7). One explanation is a shell that has persisted for long time and for some reason waves cannot consume its free energy.

Category 1: 1/4-consumed shell (Fig. 8). Our interpretation is that we are well above the region where waves consume the free energy.

Category 2: half-consumed shell (Figs. 4 and 9). Seems to be always associated with waves/anisotropies. One interpretation is that we are just on the top of the region where waves consume energy.

Category 3: 3/4-consumed shell (Fig. 10). Seems to be always associated with waves and anisotropies. One interpretation is that the observation point is inside the region where the waves consume energy.

Category 4: completely consumed shell, i.e. distribution containing no free energy but containing plateaus over some energy range.

Category 5: full ion shell together with electron anisotropy. The distribution function does not differ from Category 0 (Fig. 7), but now there are simultaneous electron anisotropies. One explanation is that a shell has persisted for a long time, but only recently have waves started to consume it somewhere below the observation altitude. Ions from the consumption region have not yet reached the observation point, but the electrons have.

Category 6: full ion shell whose downgoing part is stronger than the upgoing part (Figure 11). One interpretation is that the process that creates the shell gets strengthened with time. Otherwise this is similar to category 0 or 5.

This categorisation is not complete in the sense that every possible shell distribution would necessarily fit in one of the categories, but we have found it useful in practice.

We now mention some properties of ion shells and related Polar parameters that we have learned by looking at many plots similar to those shown in Figs. 7-11.

In the auroral region, usually the largest ion distribution free energy density occurs near the polar cap boundary, i.e. in the PSBL. This will be studied in section 7 below.

Whenever there is an ion shell (full shell or partly consumed shell), there is always an upgoing ion beam or ion conic (seen in panel e in the upper subfigures and near the centre of the distribution function subfigures). If one separates the counts in hydrogen and oxygen (plots not shown), one finds that the shell distribution is almost always purely hydrogen, whereas the upgoing beam or conic is a mixture of hydrogen and oxygen.

In cases where the polar cap boundary is clearly visible (i.e. in cases where the auroral oval does not move much when the satellite is traversing the PSBL), one often sees an ion shell with clear energy-latitude dispersion, with higher energy shells appearing closer to the polar cap boundary. This is probably a time of flight effect which has previously been identified in the literature as the velocity-dispersed ion signature (VDIS). This will be further discussed in section 8 below.

When PWI SFRA data are available, one finds that broadband features seen in EFI below 10 Hz usually correlated rather well with higher frequency broadband features in PWI frequencies (26 Hz-10 kHz). An example is seen in Fig. 9. When considering shell distribution correlation with wave activity we use the usually available EFI 1-10 Hz frequency range, but we stress that this does not necessarily imply that the waves physically coupling to the shell distribution are found below 10 Hz. It has been shown that ion shell distributions can drive unstable ion Bernstein waves in, say, 50-500 Hz frequency range (Janhunen et al., 2002).

Electron anisotropies in the auroral region usually occur in middle energies (100-1000 eV). This is seen clearly in Figs. 7 and 9. The correlation of middle-energy electron anisotropies with the auroral zone has recently been shown also statistically (Janhunen et al., 2003a).

The downgoing ion energy flux in e.g. half-consumed ion shell distributions (panel g) is often $\sim$ 15 mW m^{-2} when mapped to ionospheric plane (e.g., in Fig. 9). This is already enough to power ordinary auroral arcs.

7 Shell, wave activity and electron anisotropy correlation

We have already discussed the correlation between partly consumed shells, wave activity and electron anisotropy but will here discuss it in another form. In Figure 12 we show summary plots of ten Polar auroral zone crossings having half-consumed ion shell distributions with significant free energy densities. Each panel in the figure shows one auroral crossing, the horizontal axis being the invariant latitude. The black line in each panel is the free energy density of the TIMAS ion distribution with scale on the left. The red line is the middle-energy electron anisotropy (same as panel c in Fig. 7) with scale on the right. The green line is the EFI electric wave amplitude in the 1-10 Hz frequency range, averaged in 12 s blocks. The wave amplitude curve is normalised to its maximum, but the maximum value (mV/m) is written in each panel, as is also the maximum downward TIMAS ion energy flux (mW m^{-2}). The maximum for the downward energy flux is taken over those datapoints whose free energy density exceeds 0.02 keV cm^{-3}; usually the maximum downward energy flux occurs near the maximum free energy density (black curve). In addition, each panel contains information about the date, whether Polar is moving to the left (L) or right (R) in the plot and the UT hour, MLT and radial distance R of the centre of the crossing.

From Figure 12 one sees that usually the largest free energy densities occur in the PSBL, i.e. near the polar cap boundary. In some of the plots one also sees radiation belt shells at low ILAT. In many cases the electron anisotropies and waves correlate in a broad sense with the free energy density, at least in the sense that cases with high free energy density near the polar cap boundary (PSBL) are almost always associated with strong waves and anisotropies close to that boundary as well. Further away from the polar cap boundary one often sees anisotropies and waves without free energy density nearby, but the amplitude of the waves and anisotropies is typically less than in the PSBL.

8 Summary and discussion

The ion shells in the ILAT range 65-75 can be separated into radiation belt and auroral zone ion shells. The radiation belt ion shells differ from the auroral zone shells in many respects: they are on the average more energetic, they have wide loss-cones, they are not related to electron anisotropy or wave activity and they typically have a long duration in Polar data (wide ILAT coverage). In this paper we have concentrated on the auroral zone ion shells since they may play an important role in the energy exchange in the auroral zone. We found that most ion shells occur at the boundary to the polar cap and probably originate from the plasma sheet boundary layer (PSBL). We now summarise our main observational findings regarding auroral zone ion shells.

1. Ion shells consist almost exclusively of hydrogen only.
2. When the free energy density is significant (> 0.1 keV/cm^3), the shell is almost always close to the polar cap boundary (i.e., the PSBL) (Fig. 1 panel c).
3. If a threshold of 20 eV cm^{-3} is chosen for the free energy density, PSBL ion shells have an occurrence frequency of 5% which is comparable to the occurrence frequency of potential minima of auroral arcs (Janhunen et al., 2003b), Fig. 1 panel b.
4. Plateaued distributions which we interpret as partly or completely consumed remnants of shell distributions are common in the auroral zone.
5. Partly consumed ion shells are associated with wave activity and middle-energy (100-1000 eV) electron anisotropy (Fig. 12).
6. The total ion downward energy flux associated with ion shell distributions is ~ 15 mW m^{-2} in many events, but can be as large as 42 mW m^{-2} (Fig. 12 panel 4).
7. Although we used the frequency range 1-10 Hz to measure wave activity in most cases, higher frequencies (10-500 Hz) are also usually excited at the same time (Fig. 9 panel a).
8. A clear energy/latitude dispersion is seen, where higher ILAT corresponds to higher shell energy, until some cutoff at which the shell disappears (so-called velocity-dependent ion signature (VDIS) events).
9. PSBL ion shells are always associated with an upgoing ion beam, which typically has much smaller energy than the shell. Typically the ion beam contains both H+ and O+ in significant amounts.
10. Stable, unconsumed shell distributions are rather insensitive to Kp variations at least in the radiation belt, but plateaued distributions (consumed shells) are more widespread in the auroral region for high Kp than for low Kp (Figs. 1 and 5).
11. While the free energy density u (Fig. 1) is minimal in the auroral zone, the so-called original free energy density u_{orig} (Fig. 5) is large there.
12. The original free energy density u_{orig} is enhanced at subauroral latitudes in the postnoon sector, which probably follows from ion motion (Fig. 6).

We now discuss some of the more important physical questions that the observational results summarised above concerning auroral zone ion shells give rise to.

The PSBL ion shells usually have an energy-latitude dispersion and are probably equivalent or at least closely related to VDIS events. Consequently, their formation mechanism is probably a time of flight effect. Ions are injected from the magnetotail and at the same time they drift earthward because of the large-scale convection electric field. Energetic fast ions have little time to convect and are thus observed almost at the same field line where the injection takes place, but slow ions convect some distance earthward during their travel and are thus not observed in the same place as the high energy ions. Thus one observes a distribution where the centre is hollow, i.e. a shell distribution. The radiation belt shells are most probably not formed by this process. One possibility for their formation is the energy dependence of azimuthal drift velocity, i.e. a competition between the energy-independent $\mathbf{E} \times \mathbf{B}$ drift and the energy-dependent gradient and curvature drifts. This mechanism might also contribute to the formation of PSBL shells.

We found many cases where a shell is partly consumed (1/4-consumed, half-consumed, 3/4-consumed, etc.). At least one way to interpret a half-consumed shell, for example, is to assume that the observation point is at the upper boundary of a region where a shell-consuming wave-particle interaction takes place. Likewise, a 1/4-consumed shell corresponds to a situation where the consumption process resides at some distance below the observation point. In more complicated cases, one may need to assume also a temporal turning on or off of the consumption process. If the energy is fixed, the pitch angle of a particle tells how long time ago the particle passed through the equatorial plane: this time is shortest for zero pitch angle (downgoing) particles and longest for exactly upgoing ones (180^{o} pitch angle). The upgoing particles have mirrored below the observation point which has taken extra time. If the consumption process worked in the past but stopped some time ago, particles launched after stopping are not affected by it, and in the distribution function they are particles whose pitch angle is smaller than some limit.

What is the role of auroral zone shell distributions in powering auroral phenomena? The largest downward ion energy flux that occurred in a shell distribution was 42 mW m^{-2} and values above 10 mW m^{-2} are not rare. This is not as large as the 100 mW m^{-2} or so which is required to power the most intense substorm aurorae (and which is available from alfvénic Poynting flux in at least some of those cases (Wygant et al., 2000)), but it could be enough to power stable auroral arcs. If the ion shell distributions are part of the energy transfer chain causing auroral arcs, the whole chain would be something like the following [see also Olsson and Janhunen (2003)]:

1. Ions are energised in the magnetotail in the reconnection X-line and injected towards the Earth. If the ions are injected as field-aligned beams, the distribution function turns into a shell distribution at lower altitudes because of the mirror force.

2. At some altitude (e.g., 3-6 R_E radial distance), the combination of magnetic field and plasma conditions are such that the shell distribution becomes unstable to waves which consume its free energy. Specifically, it has been shown that ion Bernstein waves are created by a shell distribution (Janhunen et al., 2002).

3. The waves generated by the shell distribution energise middle-energy electrons (Janhunen et al., 2002, 2003a) in the parallel direction, producing a middle-energy $T_\parallel > T_\perp$ electron distribution superposed with isotropic hot (and possibly cold) electron backgrounds.

4. A downward parallel electric field is set up because otherwise the $T_\parallel > T_\perp$ type electron distribution would create a negative charge cloud at low altitudes which is not possible since the plasma must be quasineutral.

5. Since the system in long timescales must behave electrostatically, the parallel electric field must be part of a potential structure. Because the ionosphere is approximately in constant potential (the ionospheric perpendicular fields are much smaller than the strong perpendicular fields that exist in the acceleration region), the only way to close the potential contours is with a closed negative potential structure.

6. The lower part of the potential structure accelerates electrons downward and produces peaked inverted-V electron spectra at low altitude which are also the main contributors to the optical emissions. Electrons can enter the closed negative structure with the help of the abovementioned Bernstein waves.

Many parts of the process chain described above have been found to be in agreement with data or reproduced by simulations. For a recent review, see Olsson and Janhunen (2003).

Future work regarding ion shell distributions could contain the following. One should study shell distributions in the auroral field lines also above 6 R_E radial distance which was the upper limit of this study because that could tell if there is an upper altitude below which the consumption processes take place. To model shell distribution formation, test particle simulations should be carried out. Those calculations should include a full Lorentz force integrator in order to model accurately the ion motion near the X-line, although in the near-Earth region the adiabatic approximation is probably sufficient.

Acknowledgements. We are grateful to C.A. Kletzing and J.D. Scudder for providing HYDRA data, H. Laakso and F.S. Mozer for EFI data, J.S. Pickett, D.A. Gurnett for PWI data and C.T. Russell for MFE data. The work of PJ was supported by the Academy of Finland and that of AO by the Swedish Research Council.

References

Baumjohann, W., G. Paschmann and H. Lühr, Characteristics of high-speed ion flows in the plasma sheet, *J. Geophys. Res., 95,* 3801–3809, 1990.

Bingham, R., B.J. Kellett, R.A. Cairns, R.O. Dendy and P.K. Shukla, Wave generation by ion horseshoe distributions on auroral field lines, *Geophys. Res. Lett., 26,* 2713–2716, 1999.

Bosqued, J.M., M. Ashour-Abdalla, M. El Alaoui, L.M. Zelenyi and A. Berthelier, AUREOL-3 observations of new boundaries in the auroral ion precipitation, *Geophys. Res. Lett., 20,* 1203–1206, 1993.

Bosqued, J.M., M. Ashour-Abdalla, M. El Alaoui, V. Peroomian, L.M. Zelenyi and C.P. Escoubet, Dispersed ion structures at the poleward edge of the auroral oval: Low-altitude observations and numerical modeling, *J. Geophys. Res., 98,* 19181–19204, 1993.

Eliasson, L., M. André, et al., Freja observations of heating and precipitation of positive ions, *Geophys. Res. Lett., 21,* 1911–1914, 1994.

Elphic, R.C. and S.P. Gary, ISEE observations of low frequency waves and ion distribution function evolution in the plasma sheet boundary layer, *Geophys. Res. Lett., 17,* 2023–2026, 1990.

Engebretson, M.J., W.K. Peterson, J.L. Posch, M.R. Klatt, B.J. Anderson, C.T. Russell, H.J. Singer, R.L. Arnoldy, and H. Fukunishi Observations of two types of Pc-1–2 pulsations in the outer dayside magnetosphere, *J. Geophys. Res., 107,* 1451–1471, 2002.

Gurnett, D.A., et al., The Polar Plasma Wave Instrument, *Space Sci. Rev.,* edited by *C. T. Russell, Kluwer Acad., 71,* 597–622, 1995.

Harvey, P., F.S. Mozer, D. Pankow, J. Wygant, N.C. Maynard, H. Singer, W. Sullivan, P.B. Anderson, R. Pfaff, T. Aggson, A. Pedersen, C.G. Falthammar and P. Tanskanen, The electric field instrument on the polar satellite, Space Science Reviews 71, 583-596, 1995.

Janhunen, P., A. Olsson, W.K. Peterson, H. Laakso, J.S. Pickett, T.I. Pulkkinen and C.T. Russell, A study of inverted-V auroral acceleration mechanisms using Polar/Fast Auroral Snapshot conjunctions, *J. Geophys. Res., 106,* 18995–19011, 2001.

Janhunen, P., A. Olsson, H. Laakso and A. Vaivads, Middle-energy electron anisotropies in the auroral region, *Ann. Geophysicae,* in press, 2003a.

Janhunen, P., A. Olsson and H. Laakso, The occurrence frequency of auroral potential structures and electric fields as a function of altitude using Polar/EFI data, *Ann. Geophysicae,* in press, 2002b.

Janhunen, P., A. Olsson, A. Vaivads, and W.K. Peterson Generation of Bernstein waves by ion shell distributions in the auroral region, *Ann. Geophysicae,* in press, 2002.

Karimabadi, H., D. Krauss-Varban, N. Omidi, S.A. Fuselier and M. Neugebauer, Low-frequency instabilities and the resulting velocity distributions of pickup ions at comet Halley, *J. Geophys. Res., 99,* 21541–21556, 1994.

Kucharek, H. and M. Scholer, Injection and acceleration of interstellar pickup ions at the heliospheric termination shock, *J. Geophys. Res., 100,* 1745–1754, 1995.

Olsson, A. and P. Janhunen, Some recent developments in understanding auroral electron acceleration processes, IEEE Trans. Plasma Sci., in press, 2003.

Onsager, T.G. and T. Mukai, Low altitude signature of the plasma sheet boundary layer: Observations and model, *Geophys. Res. Lett., 22,* 855–858, 1995.

Press, W.H., S.A. Teukolsky, W.T. Vetterling and B.P. Flannery, Numerical Recipes in C, The art of scientific computing, 2nd ed., Cambridge, 1992.

Russell, C.T., R.C. Snare, J.D. Means, D. Pierce, D. Dearborn, M. Larson, G. Barr and G. Le, The GGS/Polar Magnetic Fields Investigation, *Space Sci. Rev.,* 71, 563–582, 1995.

Scudder, J.D., *et al.*, Hydra - A 3-dimensional electron and ion hot plasma instrument for the Polar spacecraft of the GGS mission, *Space Sci. Rev.,* **71**, 459-495, 1995.

Shelley, E.G., A.G. Ghielmetti, H. Balsiger, R.K. Black, J.A. Bowles, R.P. Bowman, O. Bratschi, J.L. Burch, C.W. Carlson, A.J. Coker, J.F. Drake, J. Fischer, J. Geiss, A. Johnstone, D.L. Kloza, O.W. Lennartsson, A.L. Magoncelli, G. Paschmann, W.K. Peterson, H. Rosenbauer, T.C. Sanders, M. Steinacher, D.M. Walton, B.A. Whalen and D.T. Young, The Toroidal Imaging Mass-Angle Spectrograph (TIMAS) for the Polar Mission, Space Science Rev., 71, 1-4, 1995.

Wygant, et al., Polar spacecraft based comparisons of intense electric fields and Poynting flux near and within the plasma sheet-tail lobe boundary to UVI images: an energy source for the aurora, *J. Geophys. Res., 105,* 18675–18692, 2000.

Zelenyi, L.M., Kovrazkhin, R.A. and J.M. Bosqued, Velocity-dispersed ion beams in the nightside auroral zone: AUREOL 3 observations, *J. Geophys. Res., 95,* 12119–12139, 1990.

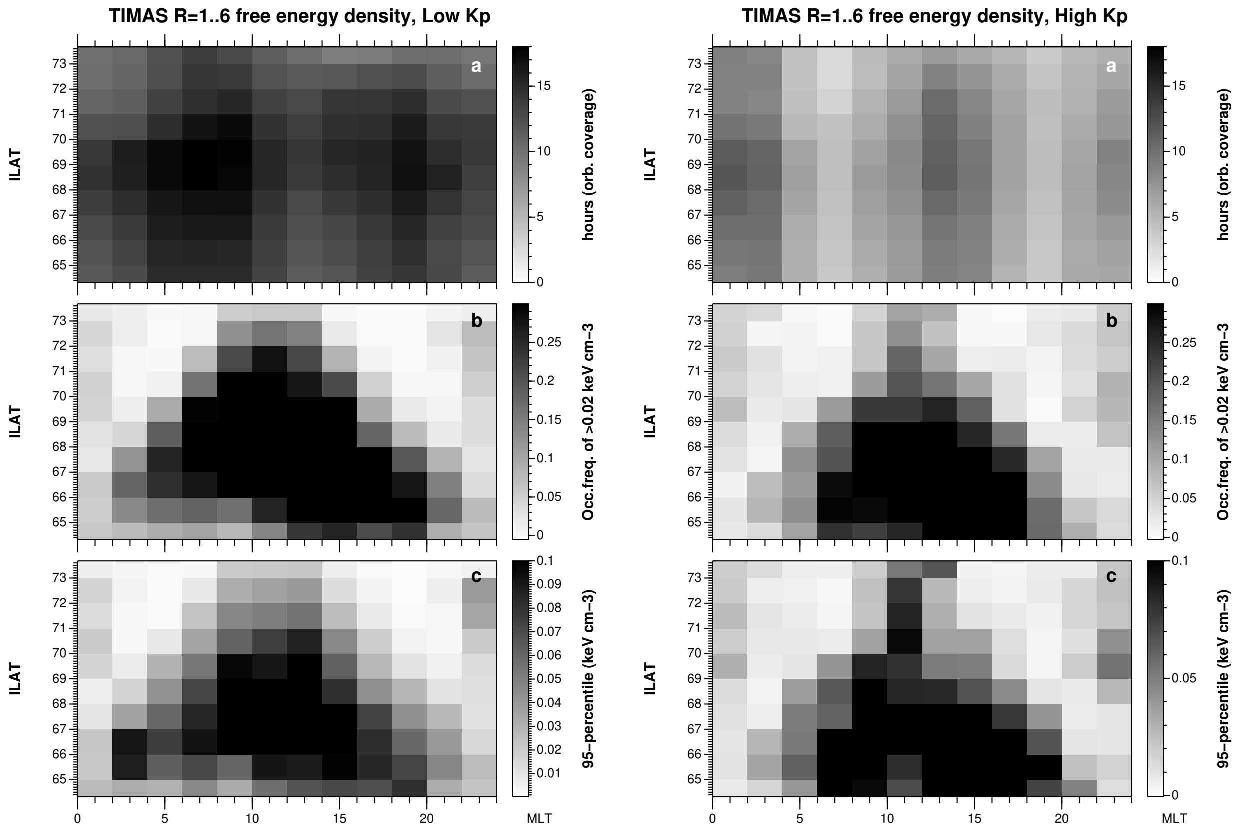

Fig. 1. Ion free energy by Polar/TIMAS as a function of MLT and ILAT for Kp ≤ 2 (left subplot) and Kp > 2 (right subplot). Radial distances from 1 to 6 R_E are included. Orbital coverage in hours in each MLT and ILAT bin (a), fraction of time the free energy exceeds 0.02 keV cm^{-3} (b), 95-percentile of free energy density (c). Some black regions are saturated.

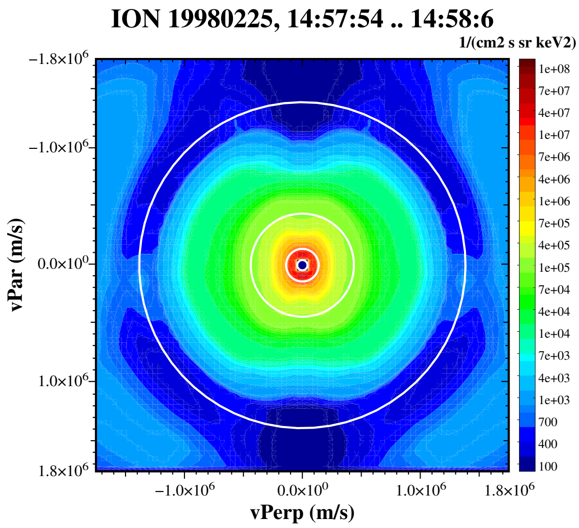

Fig. 2. Example of a radiation belt ion shell distribution. The quantity shown is the distribution function in units of $\mathrm{cm}^{-2}\ \mathrm{s}^{-1}\ \mathrm{sr}^{-1}\ \mathrm{keV}^{-2}$. Upgoing ions go up and downgoing ions down in the plot. White circles correspond to energies 10 eV, 100 eV, 1 keV and 10 keV. The shell distribution starts at ~ 15 keV and partly falls outside the plot and instrument boundaries in this case.

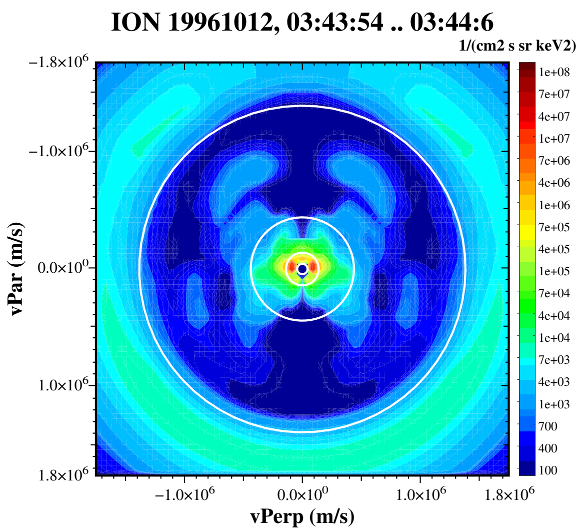

Fig. 3. Example of an event containing a full (i.e. up/down symmetric) ion shell distribution in the auroral zone. Format is similar to Fig. 2.

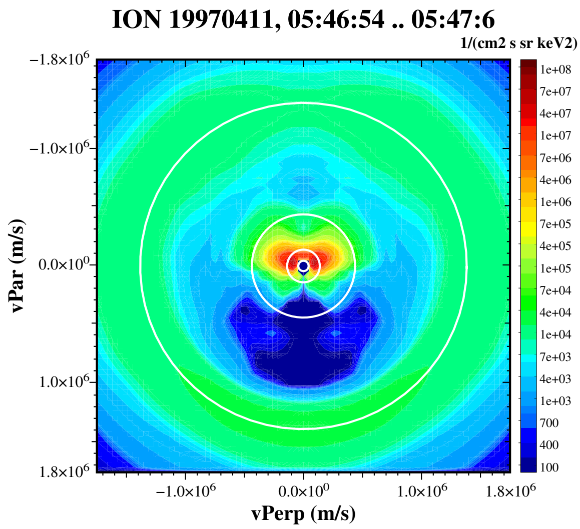

Fig. 4. Example of an event containing a half-consumed shell distribution (i.e., downgoing part is intact but upgoing part has been flattened out).

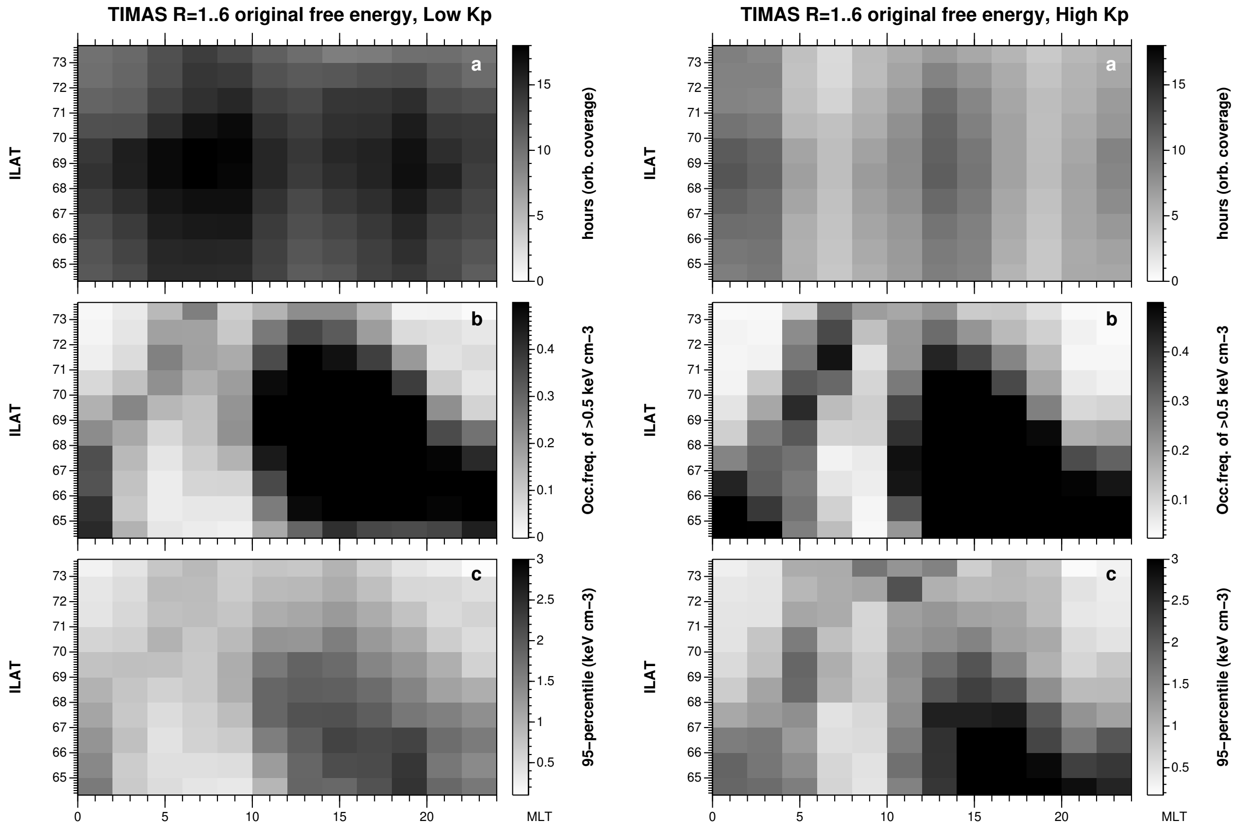

Fig. 5. Same as Figure 1 except that the quantity shown is the "original" free energy and in panel b the threshold is 0.2 keV cm^{-3}.

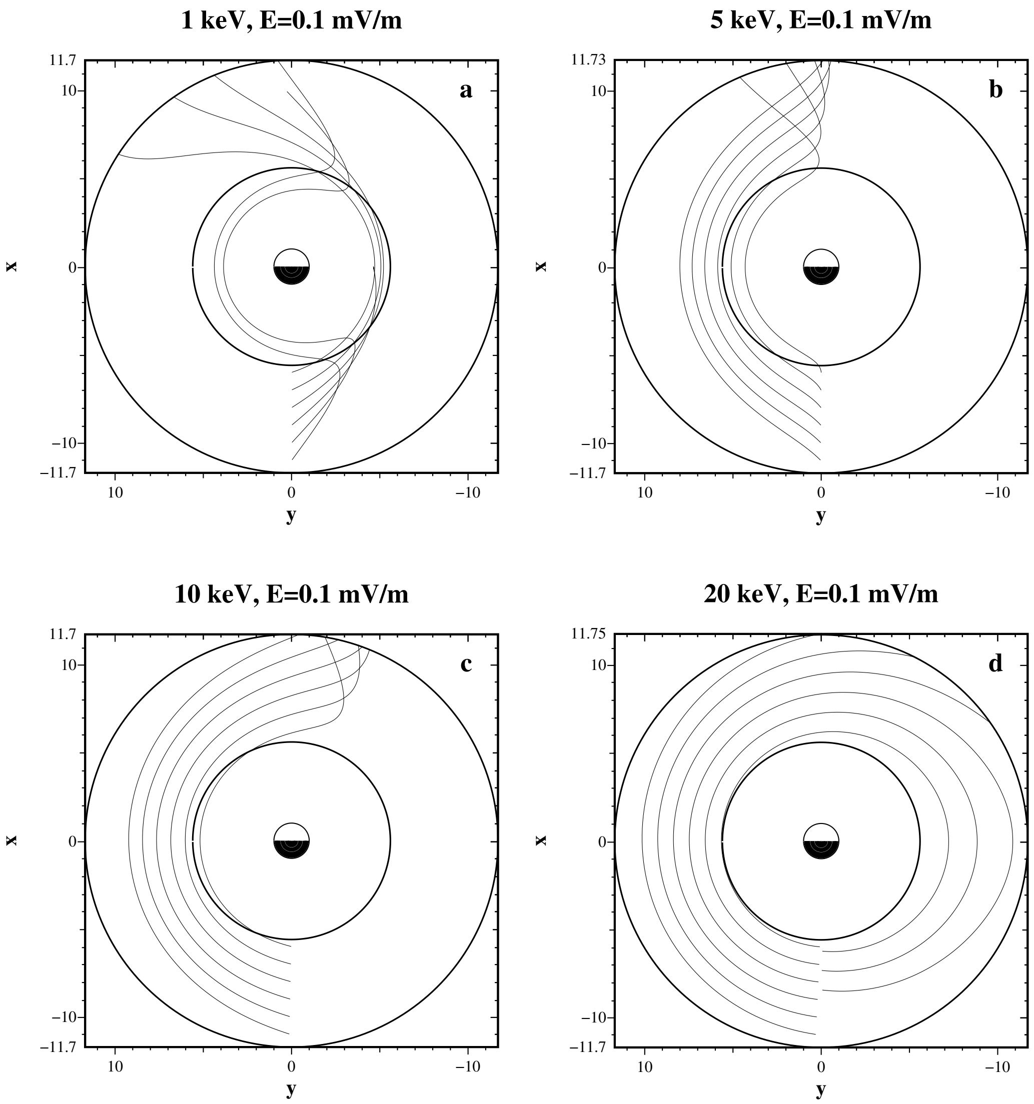

Fig. 6. Drift paths of equatorial protons launched from MLT 24 for energies 1 keV (a), 5 keV (b), 10 keV (c) and 20 keV (d). Circles corresponding to 65 and 73 ILAT are drawn, approximately corresponding to the range of data. Dipole magnetic field and a uniform duskward electric field of 0.1 mV/m are assumed.

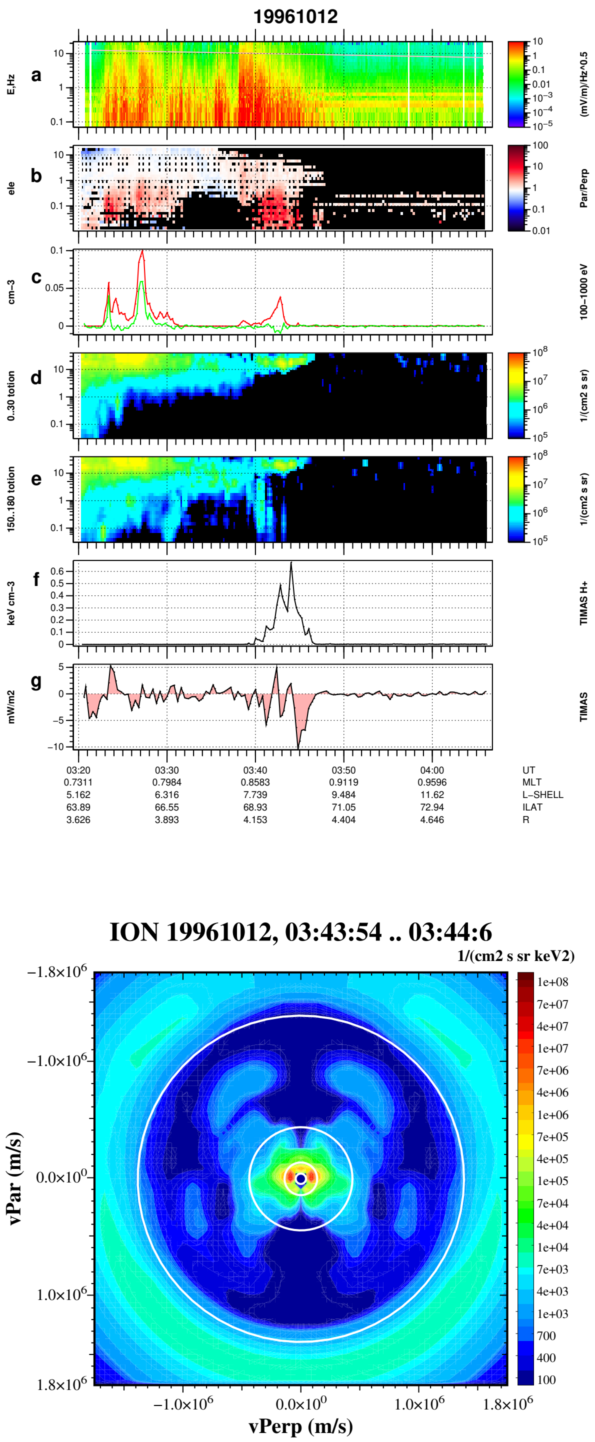

Fig. 7. Polar data for October 12, 1996, 03:20-04:08 UT. Example of an event containing a full (i.e. up/down symmetric) shell distribution. Upper subfigure: (a) EFI electric wave amplitude spectrogram, (b) ratio of parallel to perpendicular electron distribution function from HYDRA red regions signifying parallel electron energisation, (c) parallel minus perpendicular electron distribution function integrated between 0.1 and 1 keV i.e. the anisotropic density (red) and up minus down parallel component, positive meaning upgoing electrons (green), (d) total ion distribution function from TIMAS for 0-30° pitch angle i.e. downgoing, (e) same for antiparallel (upgoing) ions i.e. 150-180°, (f) free energy density in TIMAS ion distribution, (g) energy flux estimated from the free energy, positive upward. Lower subfigure: the full shell distribution, with similar format as in Fig. 2.

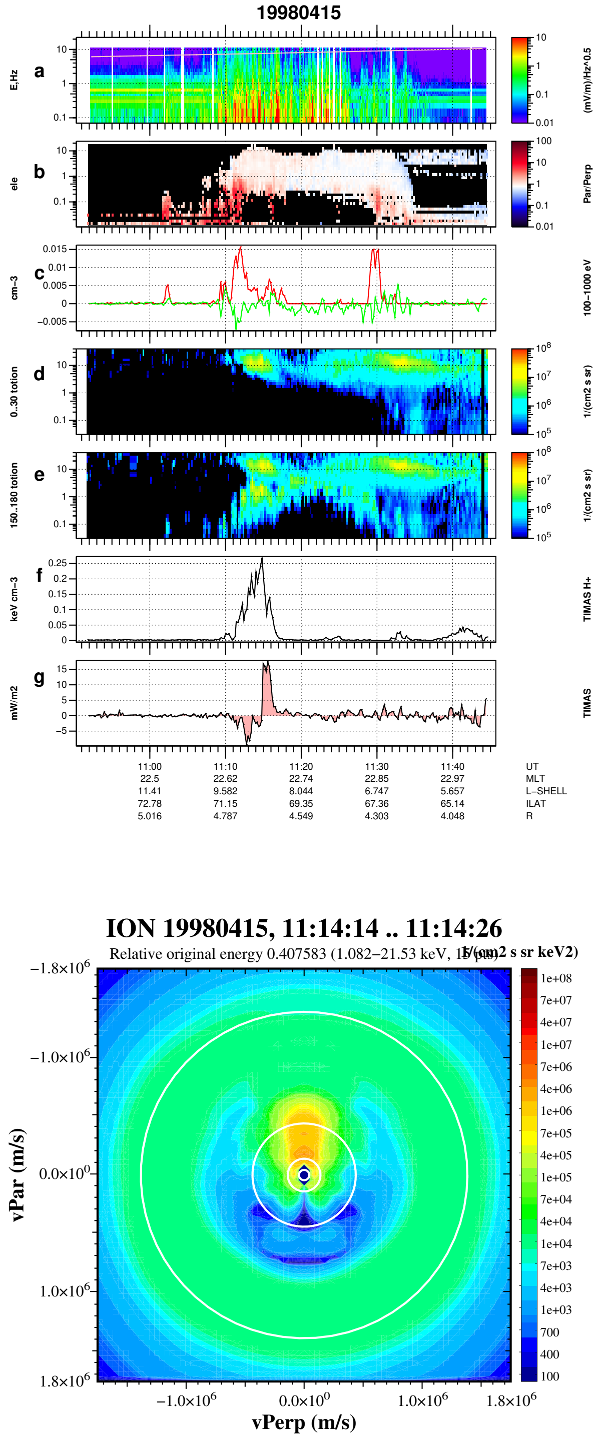

Fig. 8. Example of an event containing a 1/4-consumed shell distribution (i.e., downgoing part is intact but small pitch angles of upgoing part have been flattened out). Format is similar to Figure 2.

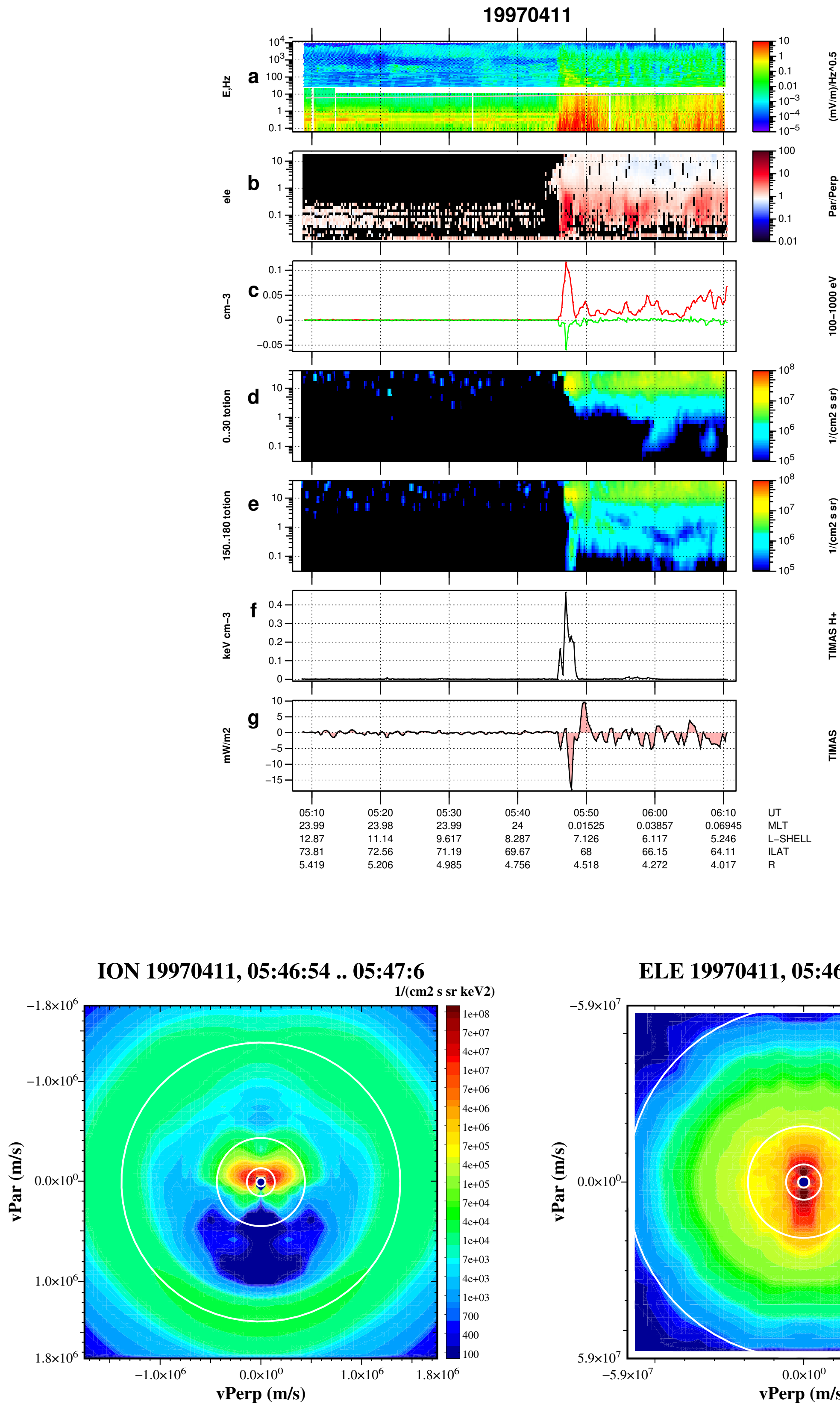

Fig. 9. Example of an event containing a half-consumed shell distribution (i.e., downgoing part is intact but upgoing part has been flattened out). In all PSBL events we have looked at there is always an upgoing ion beam embedded within the shell. Format is similar to Figure 7 except that in panel a, PWI wave data spectrogram has been added at frequencies 26 Hz-10 kHz in addition to the standard EFI spectrogram below 10 Hz.

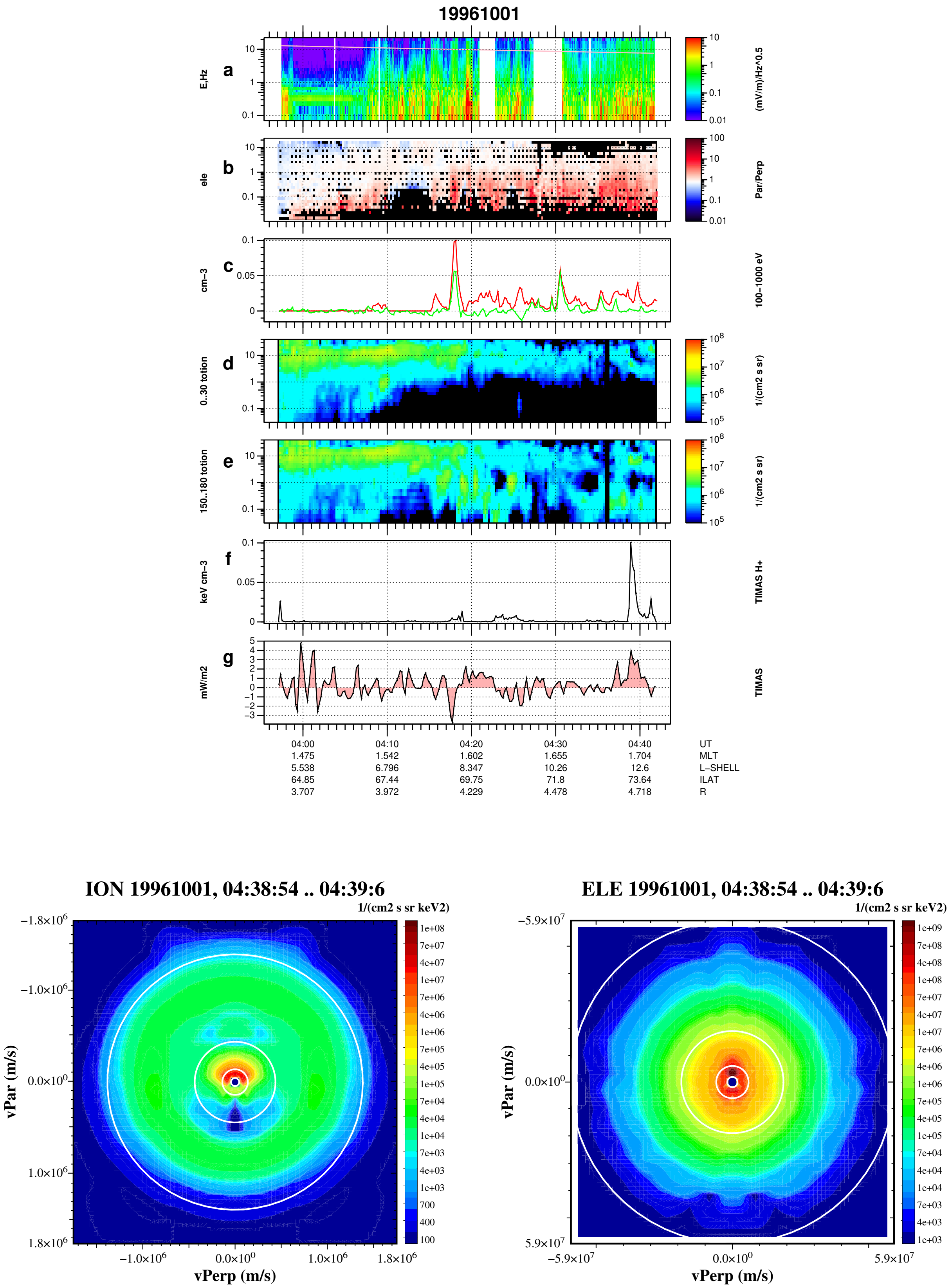

Fig. 10. Example of an event containing a 3/4-consumed shell distribution (i.e., only the small pitch-angle part of the downgoing part is intact, the rest of the distribution has been flattened out). In all PSBL events we have looked at there is always an upgoing ion beam embedded within the shell. Format is similar to Figure 7.

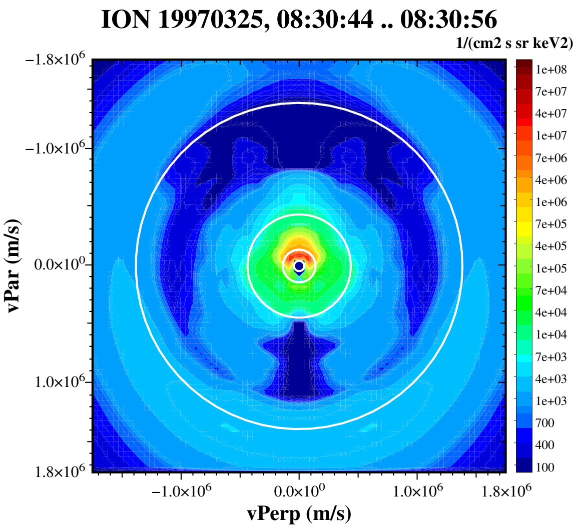

Fig. 11. Example of an event containing a full ion shell distribution whose downgoing part is stronger than the upgoing one, indicating a high-altitude source process which is becoming stronger with time. Format similar to 7.

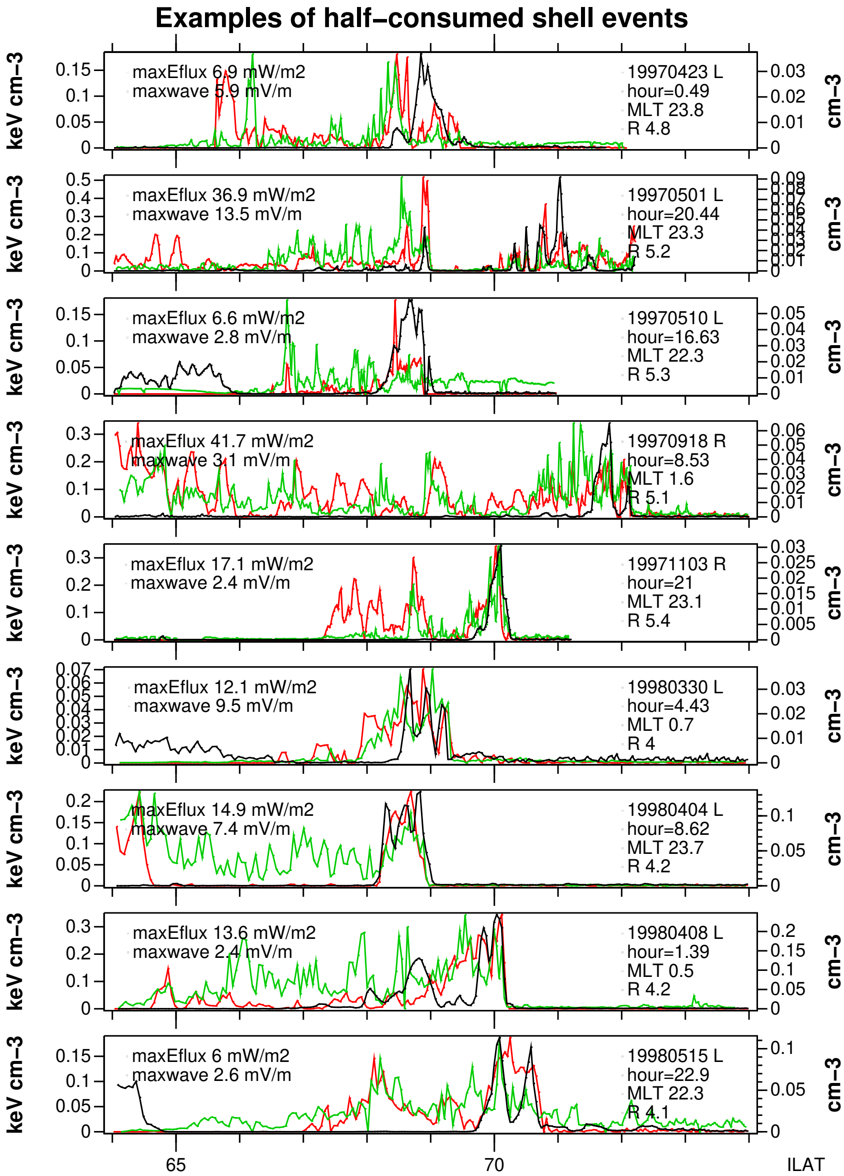

Fig. 12. Examples of half-consumed shell events. Each panel is one event. Black line is free energy from TIMAS (scale on the left) and red line is magnitude of electron anisotropy from HYDRA (scale on the right). Green line is unnormalised perpendicular wave power from EFI (12-s averaged); its attained maximum is written on the left ('maxwave'). Maximum downward ion energy flux from TIMAS during time when free energy exceeds 0.02 keV cm^{-3} is also given; the value is given at the ionospheric level by multiplying the measured value by flux tube scaling factor. Event date and average UT-hour, MLT and radial distance are also given. The letter L(R) after the date indicates that satellite is moving to the left (right), i.e. towards decreasing (increasing) ILAT.